Check for updates

View Article Online
View Journal

Nanoscale

Accepted Manuscript

This article can be cited before page numbers have been issued, to do this please use: H. Aslan, K. Kaja, J. Morán-Meza, F. Piquemal, J. Alvarez, N. Chauvin, J. Penuelas, S. M. Soenderskov and P. Regreny, *Nanoscale*, 2025, DOI: 10.1039/D4NR05107F.

This is an Accepted Manuscript, which has been through the Royal Society of Chemistry peer review process and has been accepted for publication.

Accepted Manuscripts are published online shortly after acceptance, before technical editing, formatting and proof reading. Using this free service, authors can make their results available to the community, in citable form, before we publish the edited article. We will replace this Accepted Manuscript with the edited and formatted Advance Article as soon as it is available.

You can find more information about Accepted Manuscripts in the Information for Authors.

Please note that technical editing may introduce minor changes to the text and/or graphics, which may alter content. The journal's standard Terms & Conditions and the Ethical guidelines still apply. In no event shall the Royal Society of Chemistry be held responsible for any errors or omissions in this Accepted Manuscript or any consequences arising from the use of any information it contains.

ROYAL SOCIETY OF CHEMISTRY

rsc.li/nanoscale

View Article Online
DOI: 10.1039/D4NR05107F

Open Access Article. Published on 06 March 2025. Downloaded on 3/11/2025 5:41:50 PM.
This article is licensed under a Creative Commons Attribution 3.0 Unported Licence.

1 # Atomic Force Microscopy as a Multimetrological Platform for Energy Devices

2 Hüsnü Aslan*[a], Khaled Kaja[b,f], José Morán-Meza[b], François Piquemal[b], José Alvarez[c,d], Nicolas Chauvin[e],
3 José Penuelas[e], Steffan Møller Sønderskov[a], and Philippe Regreny[e]

4 [a] Dansk Fundamental Metrologi – Danish National Metrology Institute, Hoersholm, Denmark.

5 [b] Laboratoire national de métrologie et d'essais (LNE), FR-78197 Trappes Cedex, France.

6 [c] A Université Paris-Saclay, CentraleSupélec, CNRS, Laboratoire de Génie Électrique et Électronique de
7 Paris, Gif-sur-Yvette, France.

8 [d] Sorbonne Université, CNRS, Laboratoire de Génie Électrique et Électronique de Paris, Paris, France

9 [e] Ecole Centrale de Lyon, CNRS, INSA Lyon, Université Claude Bernard Lyon 1, CPE Lyon, INL,
10 UMR5270, Ecully 69130, France

11 [f] Present address: Bruker nano surfaces & metrology, Karlsruhe, Germany

12 † Electronic Supplementary Information (ESI) available: intermittent contact, and contact mode images as
13 well as EFM, KPFM, and C-AFM images.

14

15 * Corresponding author: asl@dfm.dk
16

Nanoscale Accepted Manuscript

View Article Online
DOI: 10.1039/D4NR05107F

Open Access Article. Published on 06 March 2025. Downloaded on 3/11/2025 5:41:50 PM.
This article is licensed under a Creative Commons Attribution 3.0 Unported Licence.

17 **Abstract**

18 In this article, we present a comprehensive study utilizing Atomic Force Microscopy (AFM) as a
19 multimetrological platform for the characterization of novel energy harvesting devices, with a particular
20 focus on optical nanomaterials - nanowires. Despite their challenging structure, AFM offers exceptional
21 versatility in probing dimensional and functional properties of nanowires at the nanoscale. We demonstrate
22 the capabilities of AFM measurements to provide an extensive understanding of the structural, electrical,
23 and spectroscopic properties of nanowires using different operational modes, including Electrostatic Force
24 Microscopy (EFM), Kelvin Probe Force Microscopy (KPFM), and Conductive-AFM (C-AFM). Our
25 findings establish AFM as an invaluable metrological tool for the development of cutting-edge energy
26 harvesting technologies and optical nanomaterials.

27

28 **Keywords:** Nanowires, AFM, Metrology, EFM, KPFM, CAFM, DNM

Nanoscale Accepted Manuscript

View Article Online
DOI: 10.1039/D4NR05107F

Open Access Article. Published on 06 March 2025. Downloaded on 3/11/2025 5:41:50 PM.
This article is licensed under a Creative Commons Attribution 3.0 Unported Licence.

1. Introduction

Nanotechnology has revolutionized the field of materials science, enabling the development of novel energy harvesting devices and nanomaterials with unique properties at the nanoscale. Owing to their one-dimensional structure, nanowires have emerged as highly promising candidates for improved-efficiency devices in solar and electro-mechanical energy applications. When vertically aligned in solar cells, semiconducting nanowires expose a larger surface area for light collection compared to their film-like counterparts. Similarly in electro-mechanical transductors, vertical nanowires exhibit a favoured configuration for mechanical bending, implying a higher energy conversion efficiency. Thus, making these optical nanomaterials excellent candidates for diverse biomedical and environmental applications.

To fully utilize the scientific and commercial potential of nanowires, a comprehensive understanding of their properties is required. However, accurate characterization is complicated due to their nanoscale geometry, fragility, and complex behaviour. Atomic Force Microscopy (AFM) has emerged as a powerful metrological tool capable of probing surface properties and obtaining dimensional information with high resolution, precision and accuracy using low controllable forces.[1] Its versatility and ability to operate in various modes make it an ideal platform for investigating nanowires and advancing their associated technological applications.

AFM's scanning capabilities allow for precise imaging and measurement of nanowires' dimensions, providing crucial insights into their morphology, roughness and aspect ratio. For instance, AFM was employed to measure the diameter and length of silicon nanowires (NWs), unveiling their growth kinetics in line with their mechanical and structural properties.[2] Various AFM-based techniques were utilized to study the surface roughness of nanowires, which plays a crucial role in their electronic and mechanical properties.[3] Wang et al. investigated the surface roughness of zinc oxide nanowires, revealing the influence of growth conditions on their surface morphology and potential for device applications.[4]

Despite the importance of the nanowires' surface morphology, investigating their electrical properties plays a key role in the development of their energy-conversion functionalities. Conductive-AFM (C-AFM) and Electrostatic Force Microscopy (EFM) have been used to comprehend the electrical properties of nanowires. On one hand, C-AFM, using a continuous contact approach measures local variations in conductivity and current distribution along nanowires, aiding in the assessment of their local electronic transport properties.[5, 6] EFM, on the other hand, uses a non-contact approach to measure electrical properties related to charges distributions and local oxidation effects.[7-9] EFM was utilized to study the charge distribution of copper nanowires, highlighting the influence of surface charges on their electrical behaviour.[10] Similar to EFM, the Kelvin probe force microscopy (KPFM) method has been employed to investigate the work function and surface potential of nanowires, enabling a comprehensive understanding of their electronic properties. Singh

Nanoscale Accepted Manuscript

View Article Online
DOI: 10.1039/D4NR05107F

Open Access Article. Published on 06 March 2025. Downloaded on 3/11/2025 5:41:50 PM.
This article is licensed under a Creative Commons Attribution 3.0 Unported Licence.

62 et al. characterized single-crystalline germanium nanowires using KPFM, revealing the influence of crystal
63 orientation on their surface potential.[11]

64 Furthermore, AFM-based characterization in the radiofrequency (RF) range (not shown here) uses the
65 Scanning Microwave Microscopy (SMM) or Scanning Microwave Impedance Microscopy (sMIM)
66 methods to investigate local electrical and dielectric properties of NWs. SMM and sMIM use a conductive
67 AFM probe to transmit a microwave signal (in the gigahertz frequency range) to the sample of interest and
68 to collect the signal reflected by the sample. They enable impedance or admittance measurements at the
69 nanoscale, giving access to the electrical permittivity (dielectric constant and loss angle tangent) and dopant
70 concentration of various materials (semiconductors, dielectrics, 2D materials, quantum materials, etc.).[12-18]
71 Li et al. investigated the dopant distribution profiles of Si (n-type) and Zn (p-type) impurities within
72 individual multijunction GaAs NWs using qualitative sMIM measurements and correlated with infrared
73 scattering-type near-field optical microscopy.[19]

74 In this paper, we demonstrate that AFM can serve as a versatile and indispensable tool for the
75 multimetrological characterization of nanowires and novel energy harvesting devices. We show results
76 obtained on semiconducting NWs using various operational modes and complementary techniques,
77 demonstrating precise dimensional measurements, electrical property mapping, and spectroscopic analysis
78 in various environmental conditions. This thorough understanding of nanowire properties paves the way for
79 the development and optimization of nanoscale energy harvesting devices, contributing to the advancement
80 in the field of nanotechnology.

81

82

Nanoscale Accepted Manuscript

View Article Online
DOI: 10.1039/D4NR05107F

Open Access Article. Published on 06 March 2025. Downloaded on 3/11/2025 5:41:50 PM.
This article is licensed under a Creative Commons Attribution 3.0 Unported Licence.

83 ## 2. Material and methods

84 ### 2.1 AFM Metrology

85 Dimensional characterizations at the micro- and nanoscale are routinely conducted by calibrated AFMs
86 traceable to certified length standards. Once calibrated in the x, y, and z directions (see Fig. 1), the AFM
87 can be used for metrological purposes. AFMs comprise a head unit and a sample stage, which can move
88 independently from each other. They can be used either in a tip-scanning or a sample-scanning
89 configurations. Moreover, AFM operations can be conducted by various approaches based on the feedback
90 mechanism. Typically, three different methods are used for imaging, namely: contact mode with deflection-
91 based feedback, intermittent contact mode with amplitude modulation and deflection feedback, and non-
92 contact modes with either amplitude or frequency modulation feedback. Furthermore, force-distance or
93 force-time feedback methods can be used for dynamic nanomechanical microscopy (DNM), current or
94 contact potential feedback can be used for conductive-AFM measurements, lastly, AC and DC bias feedback
95 methods can be used for nanoelectrical measurements such as EFM and KPFM. While using AFM beyond
96 imaging two or more feedback mechanisms are employed simultaneously, for example in C-AFM while
97 deflection feedback helps measure the surface topography and ensures reliable contact for charge transport,
98 the current feedback is used to measure the resistance/conductivity of the surface. Often each method has
99 distinct advantages and disadvantages, for example contact mode is an excellent choice for hard, flat
100 surfaces and essential for any current and thermal measurements but on soft samples this method likely will
101 damage the sample and the tip. AFM as a multi-metrological platform, enables swift change between modes
102 and various feedback methods to capitalize on the advantages of each mode while overcoming or
103 compensating for their inherent limitations.

104 ### 2.1 Semiconducting nanowires

105 The fabrication of novel photovoltaic semiconductors-based energy harvesting devices aims at maximizing
106 the effective surface area of light-exposed tuneable nanostructures while ensuring that they preserve their
107 delicate form. Here, we fabricate III-V nanowires tailored for the integration in solar cells, using different
108 configurations as follows.

109 #### *2.1.1 Pure and doped GaAs nanowires*

110 Arrays of pure and doped GaAs nanowires (NW) were fabricated by Molecular Beam Epitaxy (MBE) on
111 silicon (111) substrates using the Vapor Liquid Solid (VLS) growth method[20, 21]. The first step consisted in
112 gently cleaning the substrate in acetone and ethanol, followed by a 200 °C outgassing for a few minutes to
113 remove contaminations. Subsequently, the substrate was introduced in the main chamber for further growth,
114 where its temperature was increased to 450 °C to deposit Ga liquid droplets on the surface for etching the

Nanoscale Accepted Manuscript

View Article Online
DOI: 10.1039/D4NR05107F

Open Access Article. Published on 06 March 2025. Downloaded on 3/11/2025 5:41:50 PM.
This article is licensed under a Creative Commons Attribution 3.0 Unported Licence.

Nanoscale Accepted Manuscript

115 silica native layer. Then, the substrate temperature was increased to ~600 °C to initiate the VLS growth by
116 simultaneously opening the Ga and As shutters. The crystal structure can be finally tuned by adjusting the
117 V/III ratio, which was set close to 2.4 in our case resulting in a cubic crystalline structure. By tuning the
118 growth time, we were able to control the length of the nanowires, and their diameters were modified by
119 stopping the VLS growth to switch to a radial growth mode (Fig. 2).

120 The NW doping was controlled by evaporating a foreign element during the growth, i.e., Be for p-type
121 doping and Te for n-type doping. Generally, the dopant concentration is expected to be somehow linearly
122 dependent on the dopant molecular beam flux during the VLS growth. However, the dopant incorporation
123 process is rather complex since it induces a pathway related to the dopant's incorporation in the liquid
124 catalyst droplet, followed by diffusion and nucleation at the liquid solid interface.

125 A series of vertical, p-doped and n-doped NWs were grown and then encapsulated in a Benzocyclobutene
126 (BCB) polymer matrix for ensuring their mechanical stability. The BCB matrix was etched by reactive ion
127 etching and a chemical HCl etching to expose the top surface of the NWS for further accessibility to
128 electrically contacting them during AFM conductivity measurements.

129 *2.1.2 GaAs NW PIN junction nanowires*

130 Axial GaAs PIN junctions were fabricated on Si N+ substrate by opening and closing the shutter
131 appropriately during the growth. A 200 nm long section was incorporated between the p- and n-doped
132 regions to favour carriers' separation. Fig. 3 illustrates the design of two samples fabricated with PIN
133 structures, and a typical SEM picture. First sample was fabricated without passivation while the second was
134 passivated by a 10 nm AlGaAs layer, as illustrated in the schematic representation in Fig. 3a. Both samples
135 were grown on Si(111) N+ substrate, starting with the N segment including GaAs and a vapor of Te (the
136 GaTe cell temperature was 450 °C) during 12 minutes. Then, the Te shutter was closed, and the GaAs
137 continued growing for 2.5 minutes resulting in an intrinsic segment. Subsequently, the Be shutter was
138 opened for 4.5 minutes to form the P doped segment (the Be cell temperature was 850 °C). Finally, the Ga
139 droplet catalyst was consumed, and then the radial growth was performed to protect the III-V nanowires
140 facets and avoid surface recombination, this was done by growing an AlGaAs shell at 400 °C for 4 minutes
141 on one of the two samples.

142

View Article Online
DOI: 10.1039/D4NR05107F

Open Access Article. Published on 06 March 2025. Downloaded on 3/11/2025 5:41:50 PM.
This article is licensed under a Creative Commons Attribution 3.0 Unported Licence.

143 **3. Results and discussion**

144 **3.1 Morphological investigation of embedded PIN GaAs nanowires**

145 The NWs' surface morphology was measured by a metrological AFM (NX20, Park Systems, Republic of
146 Korea) in intermittent contact mode using aluminium coated, high resonance frequency silicon probe with
147 nominal $f_{resonance}$ = 330 kHz, k = 42 N/m, guaranteed AFM tip radius of curvature < 10 nm and scan rate set
148 to 0.2 Hz (PPP-NC-HR, Nanosensors, Switzerland) to help unveiling the sample's structure. This type of
149 experiment was previously conducted to assess various nanowire characteristics including, but not limited
150 to, dimension, side-wall roughness, periodicity, and defects.[22] In this study, we have selected a challenging
151 sample to test the power and flaws of diverse probing methods. The sample is composed of vertically aligned
152 p-type GaAs nanowires which were embedded in Benzocyclobutane (BCB) polymer matrix after growth
153 for structural support then etched to expose the nanowires.

154 Due to the oxidizing nature of the GaAs surface, the sample has been thoroughly cleaned prior to scans.
155 This enables selecting appropriate areas on the sample surface to measure further in AFM electrical modes
156 (e.g., C-AFM measurements). Non-periodic nanowires with differing heights are observed in Fig. 4a which
157 is a 20×20 μm^2, 512×512 pixel image, providing essential information about nanowires alignment,
158 exposure, and mechanical stability post-etching. Three different groups of nanowires are observed
159 contributing to the topography: 1) Fully exposed nanowires sticking out of the polymer matrix, 2) partially
160 exposed or just below the surface nanowires, 3) deeply embedded nanowires. This is illustrated by a cartoon
161 in Fig. 4b. A detailed look on a 5×5 μm^2, 512×512 pixel image, rendered in 3D (Fig. 4c) helps identify
162 individual nanowires sticking out of the polymer matrix, and others exhibiting various degrees of closeness
163 to the surface. The variation in NW height, and nearest neighbour distancing result in different degrees of
164 exposure, directly impacting the electrical measurements. Some NWs may not be sufficiently exposed to
165 conduct electric current, some NWs may be too tightly packed for single entity spectroscopy, affecting
166 device performance and reproducibility.

167 **3.2 EFM investigation of embedded PIN GaAs nanowires**

168 Electrostatic Force Microscopy (EFM) measurements were performed using a platinum/iridium-coated
169 silicon probe with $f_{resonance}$ = 140 kHz, k = 7.4 N/m (PPP-NCSTPt, Nanosensors, Switzerland). Conductive
170 AFM probes enable the measurement of electrostatic force variations resulting from the charged nature of
171 sample's nanostructures. Figure 5a shows a 20×20 μm^2, 512×512 pixel, non-passivated GaAs nanowires
172 imaged in double-pass EFM mode at scan rate set to 0.2 Hz, amplitude set point 47 nm, and lift height of
173 10 nm. Owing to the extreme surface sensitivity of this mode, the bright spots on the EFM amplitude map
174 (Fig. 5b) reveal the signature of the nanowires sticking out of the BCB matrix as the charges accumulate on

Nanoscale Accepted Manuscript

View Article Online
DOI: 10.1039/D4NR05107F

Open Access Article. Published on 06 March 2025. Downloaded on 3/11/2025 5:41:50 PM.
This article is licensed under a Creative Commons Attribution 3.0 Unported Licence.

175 them. Although the remaining nanowires show a contrast variation on the surface topography map (Fig. 5a
176 and 5c), only some of the fully exposed and partially protruding ones contribute to direct changes in the
177 electrostatic force measurements with differences in individual NW charge contributions (Fig. 5b and 5c).
178 In addition to probing the electrically charged nature of the nanowires, fast, intermittent contact EFM
179 measurements provide means to investigate the surface distribution of exposed nanowires and their
180 qualitative contribution to surface potential, which is crucial for further spectroscopic measurements
181 requiring direct contact between the AFM tip and the top surface of individual nanowires.

182 **3.3 KPFM investigation of embedded PIN GaAs nanowires**

183 Kelvin Probe Force Microscopy (KPFM) extends over EFM measurements by quantifying the surface
184 potential through the measurement of the contact potential difference (CPD) using an additional feedback
185 loop to minimize the electrostatic forces stemming from work function differences between the tip and the
186 sample. The KPFM method features numerous operating variations enabling surface topography
187 measurements either in intermittent contact or peak force (PF) tapping™ modes, and surface potential
188 measurements either in an amplitude modulation (AM) or frequency modulation (FM) schemes.[23, 24] Here,
189 we conducted KPFM measurements on arrays of non-passivated GaAs PiN junctions NWs by the PF KPFM
190 approach (Fig. 6) on a Dimension Icon system (Bruker, USA) using a conductive platinum/iridium-coated
191 silicon probe (SCM PIT-V2, Bruker, USA), with k = 2.93 N/m, determined using the thermal tune method,
192 a 75 kHz fundamental resonance frequency, a 25 nm nominal tip radius, and lift height of 50 nm. This
193 operating mode consists of measuring the surface topography and mechanical properties in the peak force
194 quantitative nanomechanical mapping (PF QNM™) mode, and the surface potential in FM mode.[25]
195 Experiments were performed in dark and under illumination environmental conditions to investigate
196 possible changes in the photovoltaic properties of the nanowires. The difference in CPD measured under
197 illumination and in dark corresponds to the surface photovoltage, which can be correlated to the open-circuit
198 voltage, V_{oc}.

199 Figure 6 shows the surface topography (a, d) of the sample correlated to surface potential (b, e) and adhesion
200 (c, f) maps under illumination (top row) and dark (bottom row) conditions. The surface potential maps (b,
201 e) show a dark contrast corresponding to the surface potential of the nanowires measured in KPFM.
202 Remarkably, not all nanowires observed on the surface topography maps (a, d) show a surface potential
203 contrast (b, e). Moreover, the measured nanowires exhibit different contrast levels on the surface potential
204 maps. This observation aligns well with the observation in EFM measurements (Fig. 5), indicating the
205 dependence of the nanowires' electrostatic signature on their vertical level inside the polymer matrix (i.e.,
206 protruding or embedded – Fig. 4). More importantly, the simultaneous measurement of the mechanical
207 properties in the PF KPFM mode enables the mapping of the tip-sample adhesion, as shown in Figs. 6 (c,

Nanoscale Accepted Manuscript

View Article Online
DOI: 10.1039/D4NR05107F

Open Access Article. Published on 06 March 2025. Downloaded on 3/11/2025 5:41:50 PM.
This article is licensed under a Creative Commons Attribution 3.0 Unported Licence.

f). Owing to the extreme surface sensitivity of the measured adhesion between the tip apex and the top surface of the sample, only the exposed (sticking out from the matrix) nanowires appear as dark dots in Fig. 6 (c, f). Therefore, PF KPFM offers a valuable means to unveil correlated information on the structural and electrical properties of the nanowires in the polymer-embedded array.

Figure 7 summarizes the CPD measurements performed on individual non-passivated PIN devices (with mappings shown in Fig. 6) and passivated PIN devices (mapping not shown) under both dark and illuminated conditions (Fig. 7(a, c)). It also presents the CPD differences between these two conditions (Fig. 7(b, d). The results show that nanowires exhibit ΔPD = 93.3 mV and ΔCPD = 126.1 mV for non-passivated and passivated samples, respectively. These values indicate small V_{OC} values in both cases under white LED illumination from the AFM microscope, with the passivated nanowires exhibiting *a* ≈ 30 mV higher ΔCPD value compared to the non-passivated ones. It is worth noting that the absence of passivation exposes the top surface of the nanowires sticking out of the matrix to air, which induces GaAs oxidation effects.

3.4 C-AFM investigation of embedded PIN GaAs nanowires

The top surface oxidation of the non-passivated nanowires is directly probed in conductive-AFM (C-AFM) measurements using a conductive doped diamond probe (AD2.8AS, Adama Innovations, Ireland) in contact with the sample surface. By applying a bias voltage (V_{bias}) between the tip and the sample, the current flowing through the nanowires is measured. Current maps and current versus voltage (I-V) curves could be obtained in C-AFM scanning and spectroscopic modes, respectively.[26-29]

Initial measurements on the non-passivated GaAs nanowires revealed a lack of conductivity (i.e., zero current) due to the oxidation of the nanowires' top surface. Consequently, a surface treatment protocol was devised for oxide removal, consisting of the following steps. First, the nanowire sample is immersed in boiling acetone (65 °C for 5 minutes), then in boiling methanol (65 °C for 5 minutes). Finally, the sample is immersed in concentric HCl for 30 seconds. Deionized water is used for rinsing the sample after each step.

Subsequently, C-AFM imaging measurements were carried out, enabling the correlation between the surface topography and electrical conductivity maps at various locations, as shown on Fig. 8. The C-AFM imaging results reveal a series of important information, as follows. First, all current maps (Figs. 8 (b, c, e, f)) demonstrate that only a small amount of the nanowires in the array (i.e., compared to the number of nanowires observed on the topography map) are conductive. This provides highly valuable insights into the conductivity distribution across nanowires arrays, which is key to dictating their functional performance when integrated in full devices. The access to this information unlocks direct means to assess the effectiveness of nanowires' fabrication procedures and growth conditions. Second, the current maps show

Nanoscale Accepted Manuscript

View Article Online
DOI: 10.1039/D4NR05107F

Open Access Article. Published on 06 March 2025. Downloaded on 3/11/2025 5:41:50 PM.
This article is licensed under a Creative Commons Attribution 3.0 Unported Licence.

240 some nanowires (highlighted with blue dashed squares) that yield high current values independently of the
241 bias or illumination conditions. This points toward failed nanowires, which do not exhibit any
242 semiconducting properties.

243 Third, the comparison between the current maps in Fig. 8(b, e) reveal the effect of illumination on the
244 potential photovoltaic behaviour of the nanowires. When a V_{bias} = 2 V is applied between the tip and the
245 sample, several nanowires are consistently observed conducting current in dark and under illumination,
246 which indicates a non-photovoltaic behaviour. Nevertheless, these same nanowires disappear from the
247 current maps acquired at a V_{bias} = -2 V, which points towards a diode-like behaviour of these nanowires.
248 Interestingly, additional nanowires (highlighted with yellow dashed circles in Fig. 8e) only appear on the
249 current map under illumination at V_{bias} = 2 V, which is a signature of their photovoltaic behaviour. All the
250 above results put forward the non-homogeneity of the nanowires behaviour across the array, which promotes
251 the importance of their nanoscale characterization in correlative AFM modes to deepen the insight of the
252 individual nanowires' properties affecting the overall photovoltaic devices.

253 The aforementioned observations are further confirmed via I-V measurements performed by contacting
254 individual nanowires within the array with the conductive AFM tip. Figure 9a shows an example of a non-
255 responsive wire with a flat I-V curve, while electrically responsive nanowires are shown in the I-V curves
256 in Fig. 9(b–d). Black curves are recorded during the forward sweep (i.e., rising bias voltage), whereas red
257 curves correspond to the backward sweep (i.e., dropping bias voltage). Surprisingly, the black and red curves
258 do not overlap, which raises several questions, in particular whether the first voltage sweep does not induce
259 a change in the mechanical/electrical properties of the nanowire. Nevertheless, we can still observe a diode
260 behaviour (black curve) and a pseudo photovoltaic effect (red curve). Indeed, the pseudo photovoltaic effect
261 points out a V_{OC} with no short-circuit current I_{SC}. However, the loss of mechanical/electrical contact
262 between the AFM tip and the device could be wrongly interpreted as an open-circuit device. Furthermore,
263 it should be noted that there is likely an AFM tip shadowing effect, which could influence the I-V
264 measurement procedure. In general, the illumination reaching the nanowire device is not well-defined, as it
265 primarily comes from multiple possible sources, including the LED microscope light and the alignment
266 laser. Additionally, the size of the AFM tip may impact the illumination perceived by the nanodevice. [30, 31]

267 Although the I-V curve measurements correlate well with the C-AFM and KPFM imaging results, they
268 highlight the challenging difficulty associated with single entity I-V spectroscopy on nanoscale structures
269 under varying environmental conditions. Identifying the reasons leading to disparity between I-V curves
270 calls for a significantly large number of experimental data collected over a large number of single entities.

271

Nanoscale Accepted Manuscript

View Article Online
DOI: 10.1039/D4NR05107F

Open Access Article. Published on 06 March 2025. Downloaded on 3/11/2025 5:41:50 PM.
This article is licensed under a Creative Commons Attribution 3.0 Unported Licence.

272

273 **4. Conclusions**

274 This study highlights the exceptional versatility and efficacy of the AFM as a multimetrological platform
275 for the comprehensive morphological, electrical, and spectroscopic characterization of optical nanomaterials
276 under different environmental conditions at the nanoscale. Through the synergistic application of EFM,
277 KPFM, and C-AFM modes on nanowires, we have demonstrated the capability to probe diverse
278 nanoelectrical properties with precision and high-resolution.

279 The ability to easily switch between various modes of characterization, positions the AFM as a cornerstone
280 in metrological applications for comprehensive understanding of novel energy harvesting devices and
281 nanomaterials.

282 Future research in this field can further explore the potential of AFM as a multimetrological platform by
283 integrating emerging technologies such as AFM-IR[32, 33]. This combination allows nanoscale chemical
284 characterization by coupling infrared spectroscopy with AFM's spatial, electrical, and mechanical modes.

285 **5. Acknowledgements**

286 This research project is supported by the European Union and is funded within the scope of the European
287 Metrology Programme for Innovation and Research (EMPIR) project 19ENG05 NanoWires entitled 'High
288 throughput metrology for nanowire energy harvesting devices'
289 (https://www.ptb.de/empir2020/%20nanowires/home/). Further funding has been provided by Horizon
290 Europe, Marie Skłodowska-Curie Actions Project: ENSIGN (Ref. Nr. 101086226) and both projects were
291 co-financed by the Danish Ministry of Higher Education and Science.
292 (https://cordis.europa.eu/project/id/101086226). The authors thank the NanoLyon platform for access to
293 equipment and J. B. Goure for technical assistance.

294 **Author contributions**

295 HA, KK, JMM, FP, JA, NC, JP, STS and PR have contributed to conceptualization, data acquisition,
296 curation and analysis. HA, and FP further contributed funding acquisition, project administration,
297 supervision and writing the original draft. In addition, KK and STS contributed with writing – review &
298 editing.

299 **Conflicts of interest**

300 There are no conflicts to declare.

Nanoscale Accepted Manuscript

View Article Online
DOI: 10.1039/D4NR05107F

Open Access Article. Published on 06 March 2025. Downloaded on 3/11/2025 5:41:50 PM.
This article is licensed under a Creative Commons Attribution 3.0 Unported Licence.

301 **Data availability**

302 All data supporting this article have been published online at https://doi.org/10.5281/zenodo.14271622

303 **References**

304 1. F. J. Giessibl, *Reviews of Modern Physics*, 2003, **75**, 949-983.
305 2. S. Hoffmann, I. Utke, B. Moser, J. Michler, S. H. Christiansen, V. Schmidt, S. Senz, P.
306 Werner, U. Gösele and C. Ballif, *Nano Letters*, 2006, **6**, 622-625.
307 3. Y. Coffinier, S. Janel, A. Addad, R. Blossey, L. Gengembre, E. Payen and R. Boukherroub,
308 *Langmuir*, 2007, **23**, 1608-1611.
309 4. X. Wang, J. Song and Z. L. Wang, *Journal of Materials Chemistry*, 2007, **17**, 711-720.
310 5. D. Mikulik, M. Ricci, G. Tutuncuoglu, F. Matteini, J. Vukajlovic, N. Vulic, E. Alarcon-
311 Llado and A. Fontcuberta i Morral, *Nano Energy*, 2017, **41**, 566-572.
312 6. S. H. Pham, A. Ferri, A. Da Costa, M. M. S. Mohan, V. D. Tran, D. C. Nguyen, P. Viville,
313 R. Lazzaroni, R. Desfeux and P. Leclère, *Advanced Materials Interfaces*, 2022, **9**, 2200019.
314 7. W. Hourani, B. Gautier, L. Militaru, D. Albertini and A. Descamps-Mandine, *Journal of*
315 *Vacuum Science & Technology B*, 2011, **29**.
316 8. G. Paul, *Nanotechnology*, 2001, **12**, 485.
317 9. X. Qian, Z. Lin, L. Guan, Q. Li, Y. Wang, M. Zhang and M. Dong, *Nanoscale Research*
318 *Letters*, 2017, **12**, 257.
319 10. D. Nunes, T. R. Calmeiro, S. Nandy, J. V. Pinto, A. Pimentel, P. Barquinha, P. A. Carvalho,
320 J. C. Walmsley, E. Fortunato and R. Martins, *Thin Solid Films*, 2016, **601**, 45-53.
321 11. H. M. Singh, B. Choudhuri and P. Chinnamuthu, *IEEE Transactions on Nanotechnology*,
322 2020, **19**, 628-634.
323 12. A. Karbassi, D. Ruf, A. D. Bettermann, C. A. Paulson, D. W. van der Weide, H. Tanbakuchi
324 and R. Stancliff, *Rev Sci Instrum*, 2008, **79**, 094706.
325 13. H. P. Huber, M. Moertelmaier, T. M. Wallis, C. J. Chiang, M. Hochleitner, A. Imtiaz, Y. J.
326 Oh, K. Schilcher, M. Dieudonne, J. Smoliner, P. Hinterdorfer, S. J. Rosner, H. Tanbakuchi,
327 P. Kabos and F. Kienberger, *Review of Scientific Instruments*, 2010, **81**.
328 14. J. Hoffmann, G. Gramse, J. Niegemann, M. Zeier and F. Kienberger, *Applied Physics*
329 *Letters*, 2014, **105**.
330 15. S. Hommel, N. Killat, A. Altes, T. Schweinboeck and F. Kreupl, *Microelectronics*
331 *Reliability*, 2017, **76-77**, 218-221.
332 16. M. C. Biagi, G. Badino, R. Fabregas, G. Gramse, L. Fumagalli and G. Gomila, *Physical*
333 *Chemistry Chemical Physics*, 2017, **19**, 3884-3893.
334 17. A. Buchter, J. Hoffmann, A. Delvallée, E. Brinciotti, D. Hapiuk, C. Licitra, K. Louarn, A.
335 Arnoult, G. Almuneau, F. Piquemal, M. Zeier and F. Kienberger, *Rev Sci Instrum*, 2018,
336 **89**, 023704.
337 18. D. Richert, J. Morán-Meza, K. Kaja, A. Delvallée, D. Allal, B. Gautier and F. Piquemal,
338 *Nanomaterials*, 2021, **11**, 3104.
339 19. W. Choi, E. Seabron, P. K. Mohseni, J. D. Kim, T. Gokus, A. Cernescu, P. Pochet, H. T.
340 Johnson, W. L. Wilson and X. Li, *ACS Nano*, 2017, **11**, 1530-1539.
341 20. B. A. Joyce, *Reports on Progress in Physics*, 1985, **48**, 1637.
342 21. T. Mårtensson, M. Borgström, W. Seifert, B. Ohlsson and L. Samuelson, *Nanotechnology*,
343 2003, **14**, 1255.

Nanoscale Accepted Manuscript

View Article Online
DOI: 10.1039/D4NR05107F

344 22. H. J. Yun, Kim, S. J., Hwang, J. H., Shim, Y. S., Jung, S. G., Park, Y. W., & Ju, B. K.,
345 *Scientific reports*, 2016, **6**, 34150.
346 23. K. Kaja, A. Assoum, P. De Wolf, F. Piquemal, A. Nehmee, A. Naja, T. Beyrouthy and M.
347 Jouiad, *Advanced Materials Interfaces*, 2024, **11**, 2300503.
348 24. K. Kaja, D. Mariolle, N. Chevalier, A. Naja and M. Jouiad, *Review of Scientific Instruments*,
349 2021, **92**.
350 25. B. Pittenger, N. Erina, and C. Su, *Bruker application note AN128, Rev.*, Bruker, 2012.
351 26. A. Stern, S. Aharon, T. Binyamin, A. Karmi, D. Rotem, L. Etgar and D. Porath, *Advanced*
352 *Materials*, 2020, **32**, 1907812.
353 27. A. Alexeev, J. Loos and M. M. Koetse, *Ultramicroscopy*, 2006, **106**, 191-199.
354 28. F. Giannazzo, E. Schilirò, G. Greco and F. Roccaforte, *Nanomaterials*, 2020, **10**, 803.
355 29. H. Si, S. Zhang, S. Ma, Z. Xiong, A. Kausar, Q. Liao, Z. Zhang, A. Sattar, Z. Kang and Y.
356 Zhang, *Advanced Energy Materials*, 2020, **10**, 1903922.
357 30. C. Marchat, L. Dai, J. Alvarez, S. Le Gall, J.-P. Kleider, S. Misra and P. Roca i Cabarrocas,
358 *Nanoscale Research Letters*, 2019, **14**, 398.
359 31. R. Khoury, J. Alvarez, T. Ohashi, I. Martín, P. Ortega, G. López, C. Jin, Z. Li, Rusli, P.
360 Bulkin and E. V. Johnson, *Nano Energy*, 2020, **76**, 105072.
361 32. A. Dazzi and C. B. Prater, *Chemical Reviews*, 2017, **117**, 5146-5173.
362 33. A. Dazzi, C. B. Prater, Q. Hu, D. B. Chase, J. F. Rabolt and C. Marcott, *Applied*
363 *Spectroscopy*, 2012, **66**, 1365-1384.

364

365

366

367

368

369

370

371

372

373

374

375

376

377

Open Access Article. Published on 06 March 2025. Downloaded on 3/11/2025 5:41:50 PM.
This article is licensed under a Creative Commons Attribution 3.0 Unported Licence.

Nanoscale Accepted Manuscript

View Article Online
DOI: 10.1039/D4NR05107F

Open Access Article. Published on 06 March 2025. Downloaded on 3/11/2025 5:41:50 PM.
This article is licensed under a Creative Commons Attribution 3.0 Unported Licence.

378

379

380

381 **Figure 1.**

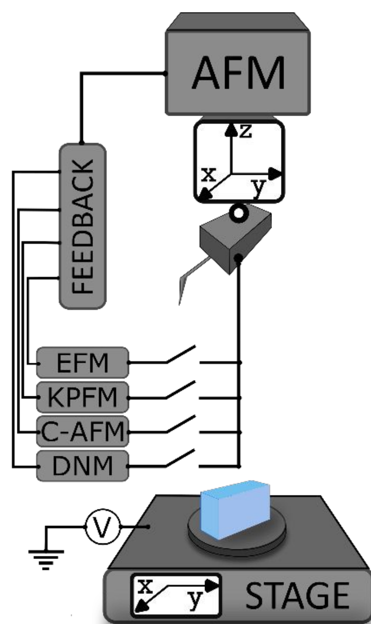

382

383 **Figure 1:** Schematic of the AFM with its calibrated x, y, z scanner head and its x, y moving sample stage,
384 as a multi-metrological platform with both tip-scan and sample-scan configurations as well as many modes
385 for nanoelectrical and mechanical characterization.

386

Nanoscale Accepted Manuscript

View Article Online
DOI: 10.1039/D4NR05107F

387 **Figure 2.**

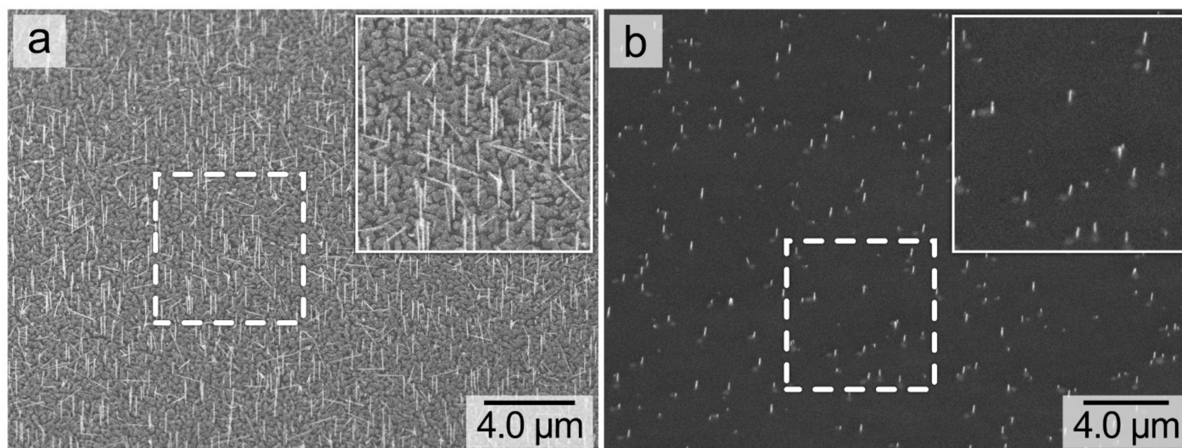

388

389 **Figure 2:** SEM images of p-type GaAs NWs after the VLS growth (a), and after the BCB encapsulation
390 and reaction ion etching revealing their upper part (b).

391

Open Access Article. Published on 06 March 2025. Downloaded on 3/11/2025 5:41:50 PM.
This article is licensed under a Creative Commons Attribution 3.0 Unported Licence.

Nanoscale Accepted Manuscript

View Article Online
DOI: 10.1039/D4NR05107F

392 **Figure 3.**

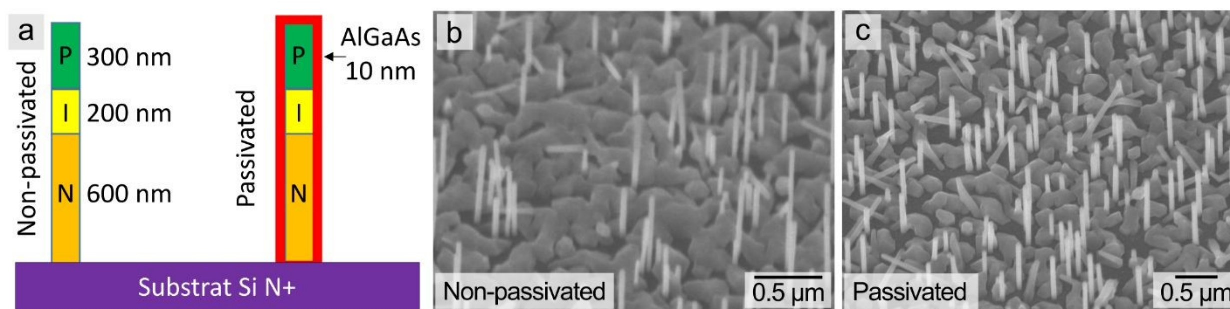

393

394 **Figure 3** (a) Drawings and (b, c) SEM images of non-passivated and passivated GaAs NW with PIN axial
395 junctions.

396

Open Access Article. Published on 06 March 2025. Downloaded on 3/11/2025 5:41:50 PM.
This article is licensed under a Creative Commons Attribution 3.0 Unported Licence.

Nanoscale Accepted Manuscript

View Article Online
DOI: 10.1039/D4NR05107F

397 **Figure 4.**

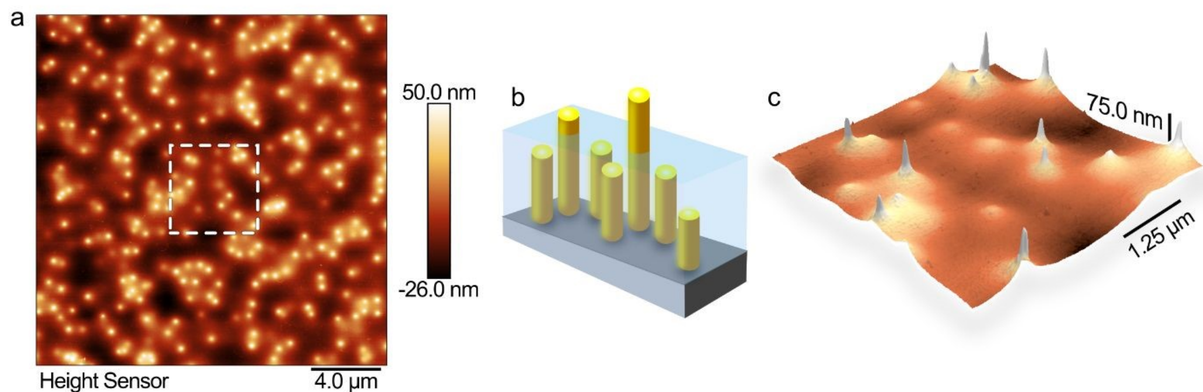

398

399 **Figure 4:** (a) A 20×20 μm^2 AFM topography image of p-type GaAs nanowires embedded in BCB polymer
400 matrix then etched. (b) Schematic illustration of the embedded nanowires highlighting the exposure of some
401 nanowires while the rest exhibits different degrees of closeness to the matrix's top surface. (c) 3D rendering
402 of the surface topography from a 5×5 μm^2 scan (dashed white square) showing various nanowires sticking
403 out of the polymer matrix, with others still fully embedded under the surface.

404

Open Access Article. Published on 06 March 2025. Downloaded on 3/11/2025 5:41:50 PM.
This article is licensed under a Creative Commons Attribution 3.0 Unported Licence.

Nanoscale Accepted Manuscript

View Article Online
DOI: 10.1039/D4NR05107F

405 **Figure 5.**

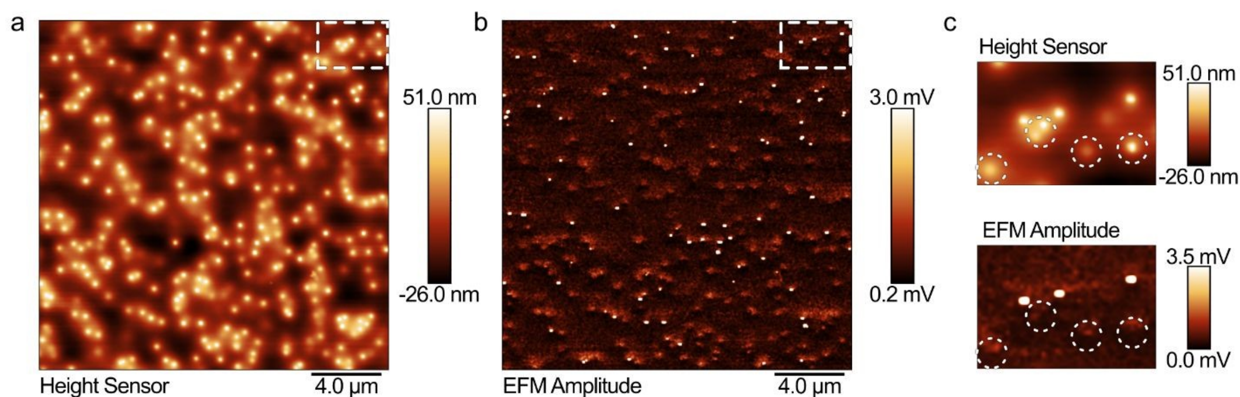

406

407 **Figure 5:** EFM measurements of non-passivated GaAs nanowires embedded in BCB polymer a) showing
408 the sample's topography and b) the variations in the EFM amplitude of the electrostatically driven oscillating
409 cantilever. Difference in individual NW contributions to surface charge is highlighted in c).

410

Open Access Article. Published on 06 March 2025. Downloaded on 3/11/2025 5:41:50 PM.
This article is licensed under a Creative Commons Attribution 3.0 Unported Licence.

Nanoscale Accepted Manuscript

View Article Online
DOI: 10.1039/D4NR05107F

411 **Figure 6.**

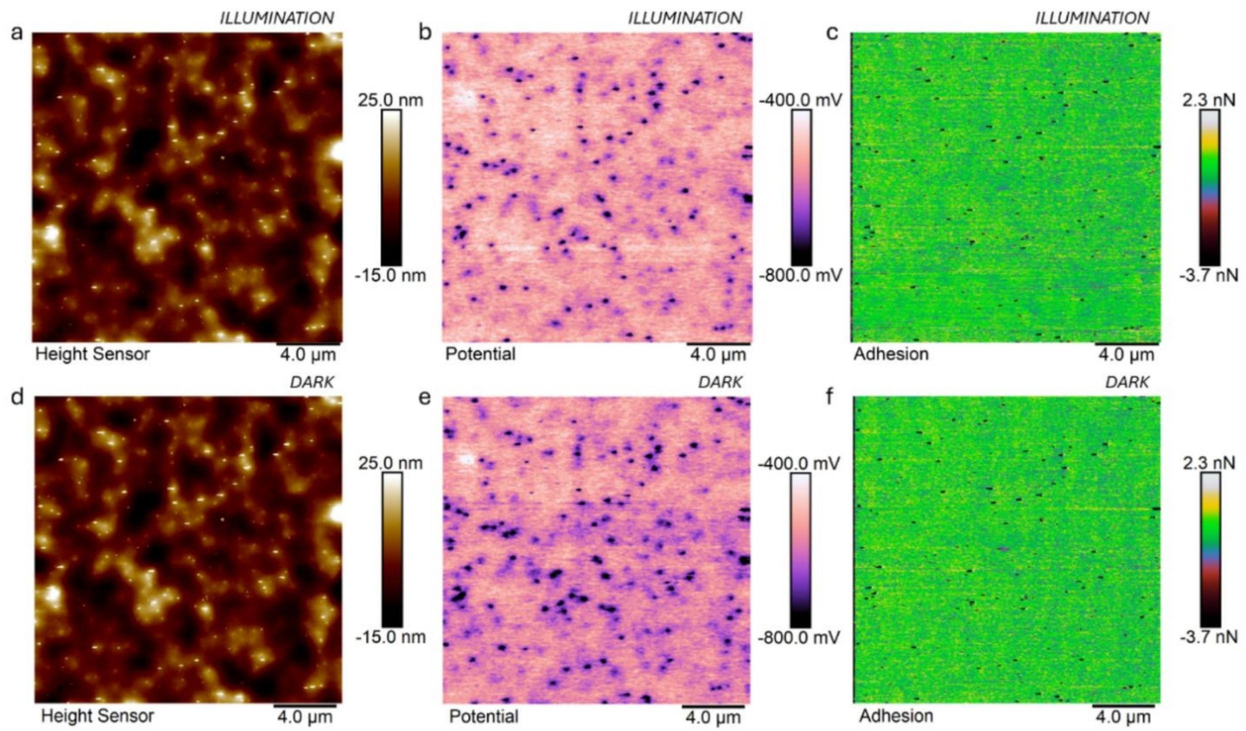

412

413 **Figure 6:** (a–c) Topography, surface potential, and adhesion maps, respectively, measured in PF KPFM
414 under illumination conditions on the sample of non-passivated vertical nanowire array (non-passivated). (d–
415 f) same measurements performed under dark conditions.

416

Open Access Article. Published on 06 March 2025. Downloaded on 3/11/2025 5:41:50 PM.
This article is licensed under a Creative Commons Attribution 3.0 Unported Licence.

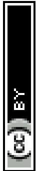

Nanoscale Accepted Manuscript

View Article Online
DOI: 10.1039/D4NR05107F

417 **Figure 7.**

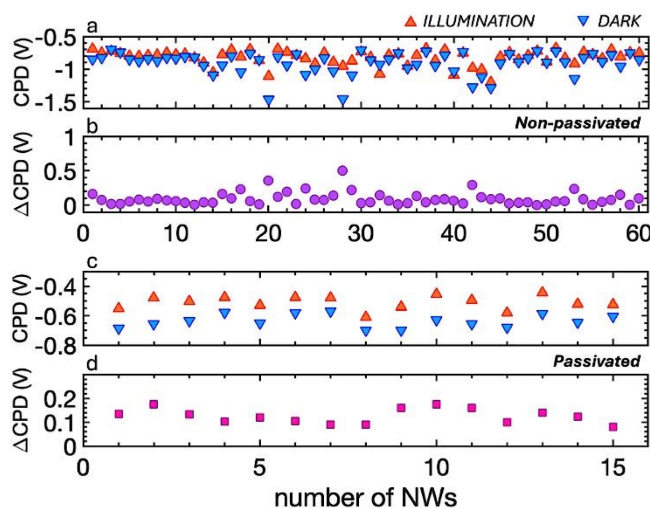

418

419 **Figure 7:** Contact Potential Difference (CPD) values measured on individual non-passivated (a) and
420 passivated (c) nanowires under illumination and dark conditions. The differences in CPD (b, d) are
421 determined for each nanowire between the measurements in these two conditions.

422

Open Access Article. Published on 06 March 2025. Downloaded on 3/11/2025 5:41:50 PM.
This article is licensed under a Creative Commons Attribution 3.0 Unported Licence.

Nanoscale Accepted Manuscript

View Article Online
DOI: 10.1039/D4NR05107F

Open Access Article. Published on 06 March 2025. Downloaded on 3/11/2025 5:41:50 PM.
This article is licensed under a Creative Commons Attribution 3.0 Unported Licence.

423 **Figure 8.**

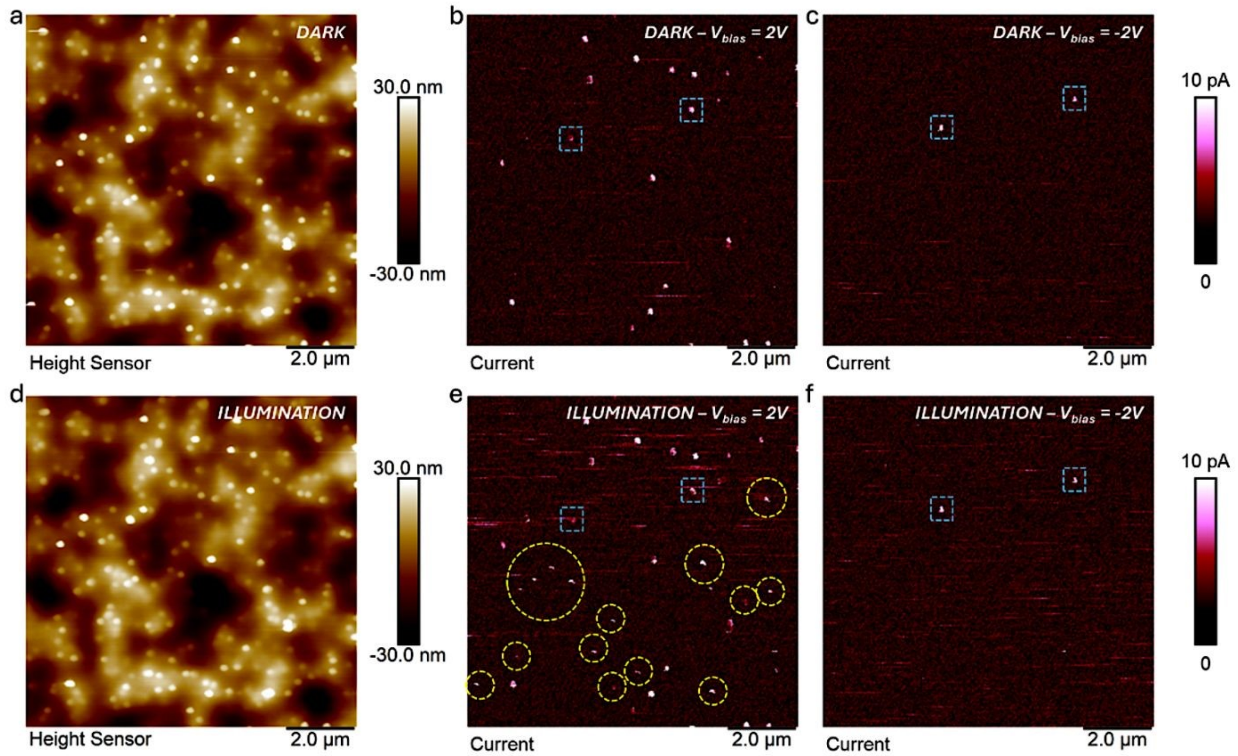

424

425 **Figure 8:** C-AFM measurements of non-passivated GaAs NWs in dark and under illumination conditions
426 showing (a, d) the surface topography maps, and current maps measured with an applied V_{bias} = 2 V (b, e)
427 and V_{bias} = -2 V (c, f).

428

Nanoscale Accepted Manuscript

View Article Online
DOI: 10.1039/D4NR05107F

Figure 9.

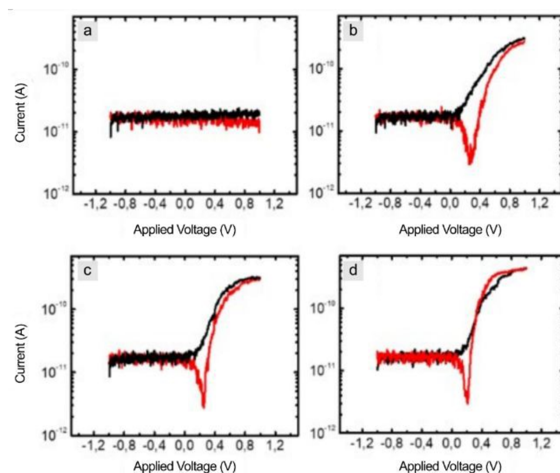

Figure 9: Current versus voltage (I-V) curves measured by contacting individual nanowires across the array. (a) example of a non-responsive nanowire. (b–d) electrically responsive nanowires showing a diode-like and pseudo-photovoltaic behaviours. Black lines correspond to the forward sweep of the bias (increasing voltage) and red lines correspond to the reverse sweep.

Open Access Article. Published on 06 March 2025. Downloaded on 3/11/2025 5:41:50 PM.
This article is licensed under a Creative Commons Attribution 3.0 Unported Licence.

Nanoscale Accepted Manuscript

View Article Online
DOI: 10.1039/D4NR05107F

Raw data for this article, including AFM, EFM, KPFM, and C-AFM images, as well as I-V spectroscopic measurements are available at zenodo at https://doi.org/10.5281/zenodo.14271622

Please note that the raw data has not yet been published. The data is under review and will be published when accepted. The submitted version can be viewed at https://zenodo.org/records/14271622?preview=1&token=eyJhbGciOiJIUzUxMiJ9.eyJpZCI6ImExYTRlNGYwLWY5NTEtNDc1Yy05YzhmLTY1ZmIyNDVmY2JlNCIsImRhdGEiOnt9LCJyYW5kb20iOiJmOTQxYWQ2MmJmMmYwMTk0NWQxMWJmN2RkMDczOWM3YyJ9.p-w-9HbT3jhqS78Jd89h-3tyfvVEEVni4jGYT6N2_Z-dH5u7Gb-sFeIcd-OBh3Tja9Cwz3YF3yGNdcinCW7e_g

Open Access Article. Published on 06 March 2025. Downloaded on 3/11/2025 5:41:50 PM.
This article is licensed under a Creative Commons Attribution 3.0 Unported Licence.

Nanoscale Accepted Manuscript